ELSEVIER

International Journal of Solids and Structures 41 (2004) 2821–2835

INTERNATIONAL JOURNAL OF SOLIDS and STRUCTURES

www.elsevier.com/locate/ijsolstr

A study of the dynamic tribological response of closed fracture surface pairs by Kolsky-bar compression-shear experiment

H. Huang, R. Feng *

Department of Engineering Mechanics, University of Nebraska-Lincoln, W316 Nebraska Hall, 900 N. 17th S., Lincoln, NE 68588-0526, USA

Received 2 January 2004; received in revised form 2 January 2004

Available online 27 February 2004

Abstract

The Kolsky torsion bar technique has been utilized successfully to develop a new compression-shear recovery experiment for dynamic tribometry of closed fracture surface pairs. This new experimental design enables combined dynamic compression and shear loading and preserves the residual specimen surface after a single cycle of loading. The experimental design was first verified through a series of dynamic friction experiments on flat 7075-T6 aluminum alloy surface pairs. The technique was then applied to study the dynamic tribological response of closed fracture surface pairs of the same material in conjunction with surface topography examination. It was found that the pre-sliding response depends primarily on normal stress and roughness of as-fractured surface. The response after the initiation of frictional sliding displays an exponential decay with increasing sliding displacement. The long-time steady-state response (if achieved) depends predominantly on normal stress. The results also show that a sufficiently high normal stress may suppress frictional sliding between the fracture surfaces giving rise to a dynamic plastic deformation continuous across the interface. An empirical model describing the key experimental observations is proposed and evaluated against the experimental data. The implication of the findings on shear cracking under high confining stress is discussed.

Keywords: Kolsky torsion bar; Compression-shear recovery experiment; Dynamic tribometry; Tribological response of closed fracture surfaces; Fracture surface topography

1. Introduction

A good understanding of the dynamic tribological response of closed fracture surface pairs is critically important for analyzing shear cracking in materials subjected to multiaxially compressive loadings.

* Corresponding author. Tel.: +1-402-472-2384; fax: +1-402-472-8292/372-8292.
E-mail address: rfeng1@unl.edu (R. Feng).

0020-7683/$ - see front matter © 2004 Elsevier Ltd. All rights reserved.
doi:10.1016/j.ijsolstr.2004.01.005

Although fracture mechanics models assuming linear Coulomb friction between a pair of closed fracture surfaces have been proposed (Margolin, 1984; Theocaris et al., 1993; Rajendran, 1994; Espinosa, 1995; Wright, 1998), there is a lack of direct experimental measurements to validate the model assumption and to determine the tribological parameters. Conventionally, the frictional resistance and wear of a tribo pair are characterized in terms of steady-state or averaged response (often over a period of repetitive frictional sliding) (Suh, 1986). The characterization of the tribological response of a closed fracture surface pair requires tribometric measurement of the *transient response* and, in case of strong dependence on surface topography, measurement of *surface evolution* (wear) during a single rapid stroke of frictional sliding. This is because shear cracking is a dynamic process even under a macroscopically static loading and the sliding between a pair of crack surfaces during the process is small (compared to that of a usual dynamic friction event) and unidirectional.

Recently, several studies have been conducted by Prakash and Clifton (1993), Ogawa (1997), Espinosa et al. (2000) and Rajagopalan and Prakash (1999) to develop experimental techniques for dynamic tribometry of flat surfaces. In the work by Prakash and Clifton (1993) and Prakash (1995), the pressure-shear plate impact technique was utilized for time-resolved measurements of the transient frictional response of highly compressed flat-surface contacts at nanosecond resolution. The other efforts were focused on extending the Kolsky (or split-Hopkison) bar technique for dynamic tribometry at microsecond resolution but for much longer time duration. Ogawa (1997) modified the Kolsky compression bar technique so that the output bar, which in the conventional usage is stationary prior to dynamic compression loading, is in a motor-driven rotation to provide a sliding motion between a specimen bonded to the output bar and another one bonded to the rotationally passive input bar. The initial relative position of the tribo pair is however not controllable. This deficiency was removed in the dynamic tribometers based on the Kolsky *torsion* bar (KTB) technique modified to include an additional axial loading unit (Espinosa et al., 2000; Rajagopalan and Prakash, 1999). Espinosa et al. (2000) reported a KTB tribometer, in which the tribo pair is subjected to a static compression and then a superposed dynamic sliding. The KTB tribometer reported by Rajagopalan and Prakash (1999), on the other hand, uses combined dynamic compression and shear. Though not pursued in these earlier studies, the initial relative position of the tribo pair can, in principle, be well controlled. This is crucial if the *conforming engagement* of a topographically complex tribo pair is imperative as for characterizing the dynamic tribological response of closed fracture surface pairs. Also, for a flat-surface tribo pair, the influence of topographical evolution of the tribo pair interface on its dynamic frictional response during a KTB tribometric experiment is expected to be small and can be reasonably neglected. However, for an engaged fracture-surface tribo pair, the topographical evolution of the interface due to wear may have a significant influence on its dynamic response. The correlation between the two needs to be considered.

To address these issues, we have developed a method that combines a specially designed KTB tribometric experiment with non-contact topographical examinations of the initial and post-test specimen surfaces. The unique feature of the new experimental design is that it enables a tribo pair to be subjected only to a *single* stroke of rapid shear. The surface topography of the tribo pair at the end of a well-defined loading cycle is preserved. Comparison of optical topographical scans of the initial and post-test specimen surfaces provides a determination of the amount and primary mechanism of interfacial wear. This method has been applied to investigate the dynamic tribological response of closed fracture surface pairs of 7075-T6 aluminum alloy. As a comparison study, the dynamic frictional response of flat-surface tribo pairs of the same material has also been measured. In what follows, details of the experimental principles and procedure will be described first. The experimental results will then be presented along with relevant discussion. Finally, a phenomenological tribological model for the closed fracture surface pairs will be presented and compared with the experimental data.

2. Description of experiment

2.1. Dynamic tribometric experiment

The experimental technique used in this work is based on a modified Kolsky torsion bar (KTB) apparatus. Details of the conventional KTB experiment were described elsewhere (Hartley et al., 1985). The modification for the dynamic tribometry of interest involves the addition of a hydraulic axial loading unit. Fig. 1 shows schematic views of the resulting KTB tribometer and the configuration of specimen, a tribo pair with an annular interface. The long circular input bar is made of 7075-T6 aluminum alloy (7075-T6 Al) and the circular output bar 4140 steel (Fig. 1(a)). The tribo pair is sandwiched between the two bars and high-strength epoxy is used to glue the tribo pair to the bars. The front end of the input bar carries a torque driver (pulley) and is coupled to the piston of the axial loading unit. The key component of the device is a friction clamp based on Duffy's design (Fig. 1(b), Hartley et al., 1985). It is capable of holding the input bar when its loading segment (between the pulley and clamp) is subjected to applied torques up to 500 N m and applied axial forces up to 32 kN *combined*. The experimental procedure is to apply torsion and compression after the clamp is activated. A forced break of a pre-notched bolt that locks the clamp (Fig. 1(b)) releases the elastic strain energy stored in the loading segment suddenly, giving rise to a pair of loading stress waves—an axial compression wave and a trailing torsion wave—propagating in the input bar downstream towards the tribo pair as well as a pair of partial release waves traveling back into the loading segment. Fig. 2 illustrates schematically the time histories of the front positions of the waves that are important to the experiment. The loading waves incident on the tribo pair are partially transmitted and partially reflected. The amplitudes of the compression and torsion waves transmitted through the tribo pair are proportional to the normal and frictional forces at the interface, respectively. The additional wave fronts at later times are due to the interactions of the waves with the bar ends. Note that the reflections of initial rarefaction waves from the pulley end are the unloading waves. Also, in circular metal bars, an elastic longitudinal (axial compressive or tensile) wave travels approximately twice as fast as an elastic torsion wave. As a result, the annular interface of the tribo pair is subjected to an incident compression at an initial time t_1 and a superposed shear at a later time t_2 (Fig. 2). Simultaneous releases of compression and shear start at t_3, the

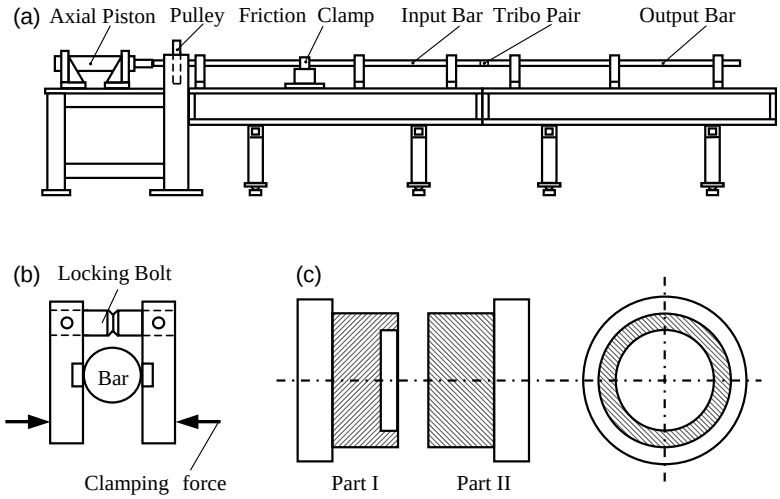

Fig. 1. Schematic view of experimental set-up and specimen configuration: (a) KTB Dynamic tribometer, (b) details of friction clamp and (c) configuration of specimen-tribo pair.

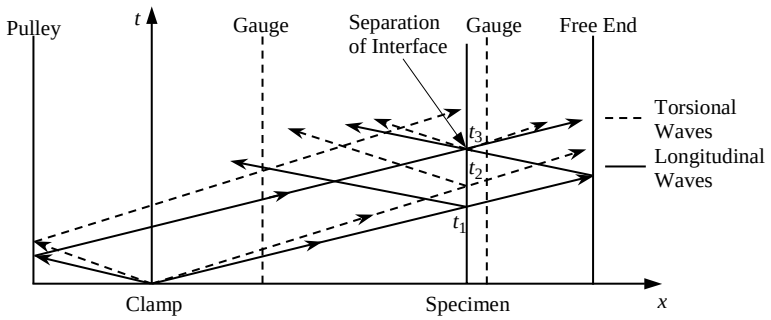

Fig. 2. Propagation (distance–time) diagram of various wave fronts during the experiment.

time when the two longitudinal unloading waves (one traveling in the input bar and the other the output bar) arrive at the interface of tribo pair. The details will be elaborated later.

The direct measurements obtained during a KTB tribometric experiment are the profiles of the stress waves incident on, reflected from and transmitted through the tribo pair. These wave profile signals are then analyzed to determine the dynamic loading conditions and the response of the tribo pair. The loading conditions are measured in terms of the nominal (averaged) normal stress $\bar{\sigma}$ and the nominal shear-sliding velocity $\bar{v}$ imposed on the annular tribo pair interface (Fig. 1(c)) while the response of the tribo pair is measured in terms of the nominal shear stress sustained by the interface $\bar{\tau}$. Specializing the Kolsky bar analysis (Hartley et al., 1985; Lindholm, 1964) for the current experimental configuration gives the following equations for data reduction:

$$\bar{\sigma} = \frac{R_2^2 E_2}{b^2 - a^2}\,\varepsilon_t, \tag{1}$$

$$\bar{v} = \frac{a+b}{2}\left[\frac{c_{s1}(\gamma_i - \gamma_r)}{R_1} - \frac{c_{s2}\gamma_t}{R_2}\right], \tag{2}$$

and

$$\bar{\tau} = \frac{3R_2^3 G_2}{4(b^3 - a^3)}\,\gamma_t, \tag{3}$$

where subscripts 1, 2, i, r, and t denote the quantities associated with the input bar, output bar, incident torsion wave, reflected torsion wave, and transmitted axial or torsion wave, respectively, R's are the radii of the bars, a and b are respectively the inner and outer radii of the tribo pair interface (Fig. 1(c)), ε_t is the axial strain associated with the transmitted compression wave, γ's are the shear strains associated with the torsion waves, E_2 and G_2 are the Young's and shear moduli of the output bar material, respectively, and c_s's are the shear wave speeds in the bar materials.

In the work reported herein, longitudinal and shear strain gauges in the Wheatstone bridge circuitry were used on each of the bars as the longitudinal and torsion sensors, respectively. A multi-channel, differential-input, digital oscilloscope operated in common-mode rejection and at a rate of 10 million samples per second was used to record the profiles of the stress waves propagating in the bars. A window-based PC workstation with NICOLET Proview software was used for data acquisition.

Depending on whether the entire bar-specimen system is compressed *before* the clamp is activated as in the work of Espinosa et al. (2000) or the loading segment of the input bar is compressed *after* the clamp is activated as in the current work, the loading mode of the KTB tribometer can be a rapid shearing-sliding either superposed on a *static* compression or a *dynamic* one. The later is more advantageous particularly for

the purpose of the current work. Under a static compression, the machining and alignment errors of the bars and tribo pair may result in a significantly uneven contact at the tribo pair interface (Espinosa et al., 2000). Accurate machining and alignment are critical to the validity of the experiment. The difficulty can be alleviated by using the combined dynamic compression and shear. With the aid of a fixture, the tribo pair can be aligned together and with *one* of the bars (say, the input bar). If the tribo pair and the output bar are kept free from any pre-stress and unwanted movement before the arrival of compression wave and the gap between the two (if any) is filled with epoxy, the initial alignment will essentially be kept during the experiment because the overall loading time (approximately 0.5 ms) is too short for the tribo pair to undergo a significant tilt. This is particularly useful for fracture-surface tribo pairs, for which the evenness of initial contact relies mostly on alignment.

The dynamic compression loading mode also facilitates the use of the mechanical impedance mismatch between the input bar (7075-T6 Al) and the output bar (4140 steel) to increase, under a given incident pulse, the effective compression force on the specimen by 40%. More importantly, the loading mode permits the use of a special experimental design to ensure that the tribo pair interface is subjected only to a single cycle of well-defined loading (compression, superposed shear, and then simultaneous unloading), and that the surface topography of the tribo pair at the end of the loading cycle is preserved for further examination. Specifically, the clamp position and the output bar length are carefully chosen so that the arrival of the longitudinal unloading wave from the input bar at the tribo pair coincides with that of the rarefaction wave resulted from the reflection of transmitted compression wave at the free end of the output bar (Fig. 2). The interaction of the two results in a rapid disengagement of the tribo pair so that the axial and shearing releases of the tribo pair occur simultaneously. It has been verified experimentally that the gap between the separated parts increases monotonically afterwards, thus preventing the two from unwanted post-test rubs that would otherwise occur due to the wave reverberations in the bars.

2.2. Specimen preparation

Two types of specimens were used in this work: usual flat-surface tribo pairs and tribo pairs formed with as-fractured surfaces. For the purpose of verifying the experimental design, the sample material was chosen to be the same as the input bar (7075-T6 Al) so that the dynamic mechanical coupling between the two was the best. The material also happens to have the mechanical properties suitable for producing rough fracture surfaces. All specimens were prepared from a 25 mm diameter, 7075-T6 Al rod. For each flat-surface tribo pair, the two components were first machined to the configuration shown in Fig. 1(c). The surfaces for testing were further lapped flat with fine silicon carbide sand paper. The average roughness (see Section 2.3 for definition) of the finished surfaces is 3.4 μm. Each fracture-surface specimen was prepared by first breaking a bolt pre-notched circumferentially with a tensile machine and then cutting off the outer edge and central portion of one of the fracture surfaces to form an annular ring. The typical inner and outer diameters of the ring are 8.2 and 11.7 mm, respectively.

2.3. Surface topography examination

For each fracture-surface tribo pair, both the initial as-fractured surface and the post-test residual surface were examined using a Proscan 1000 system, a non-contact optical profilometer capable of large-area three-dimensional (3-D) surface scanning at a resolution of 0.1 μm. In Fig. 3, the 3-D surface scans of one of the specimens before (a) and after (b) the test are shown as an example. The data from the 3-D profilometry were further analyzed to determine an asperity-volume-weighted surface roughness R_v as the representative surface topography parameter. The definition of R_v is an extension of that of the usual asperity-area-weighted surface roughness R_a based on two-dimensional line scanning measurement. In the 3-D extension, a reference *plane* is determined such that the volume enclosed between the plane and the

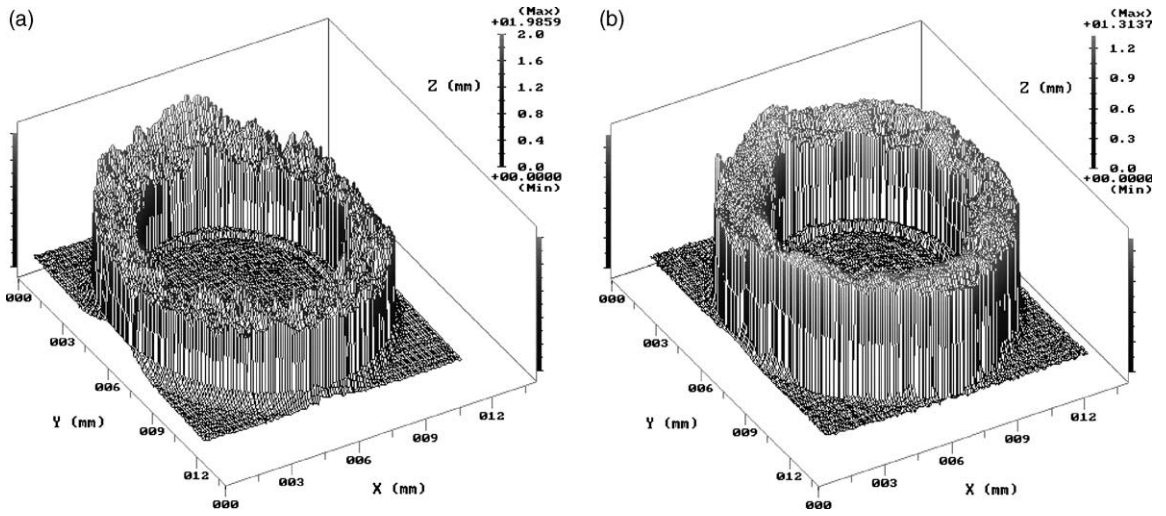

Fig. 3. Three-dimensional topographical scans of the as-fractured and tested surfaces of a tribo pair: (a) surface topography before the test ($R_v = 130$ μm) and (b) surface topography after the test ($R_v = 90$ μm).

measured surface above equals to that below. Weighted by the enclosed volume, the averaged absolute value of deviation of the surface from the reference plane gives R_v. For example, the scan of the as-fracture surface shown in Fig. 3(a) yields $R_v = 130$ μm while that of the residual surface after the test (b) gives $R_v = 90$ μm. More detailed asperity statistics can also be determined from the 3-D scan data. By comparing the surface measurements before and after the test, the topographical information useful for identifying the primary mechanism of tribo surface wear during the experiment was obtained and the amount of wear was measured.

3. Results and discussion

3.1. Results on flat-surface tribo pairs

A series of eight KTB tribometric experiments was carried out first on the flat-surface tribo pairs. Since the dynamic tribological response is expected to be relatively simple and linear according to the earlier studies on flat metallic surface pairs (Prakash and Clifton, 1993; Prakash, 1995; Espinosa et al., 2000), this series of experiments was intended to verify the experimental design and to fine-tune the new tribometer. Fig. 4 presents the time-resolved results from a typical experiment in this series. It can be seen that the compression loading is seen to arrive at the tribo pair first giving rise to a rapid increase in $\bar{\sigma}$ (the nominal normal stress, the solid line with respect to the left axis) to a plateau value of 173 MPa over a rise time within 100 μs. A similarly rapid increase in $\bar{v}$ (the nominal shear-sliding velocity, the dot-dashed line with respect to the right axis) due to the arrival of the torsion loading occurs at approximately 240 μs behind the compression. For a period of about 150 μs after the rise time, $\bar{v}$ remains at a nearly constant value of 2.42 m/s. In response, $\bar{\tau}$ (the nominal shear stress, the dashed line with respect to the left axis) first increases rapidly with $\bar{v}$ due to the static friction at the interface. However, it peaks and then relaxes quickly to a steady state before the end of the initial rise of $\bar{v}$ indicating the initiation of frictional sliding. The fact that $\bar{\tau}$ changes little during the transition of $\bar{v}$ from its later part of rising to its plateau shows clearly that the steady-state kinetic friction response of the tribo pair has very weak sensitivity (if any) to $\bar{v}$.

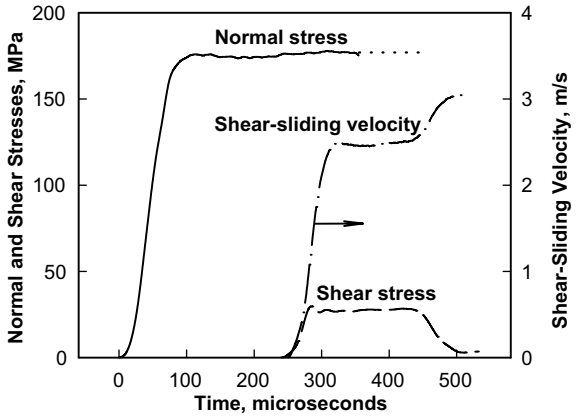

Fig. 4. Typical time-resolved tribometric measurements on flat-surface tribo pair.

By design, simultaneous releases in $\bar{\sigma}$ and $\bar{\tau}$ should appear at approximately 430 μs after the initial loading. However, only the latter is visible in Fig. 4. The special design used for achieving a single stroke of frictional sliding (see previous section) gives rise to a wave interaction at the longitudinal strain sensor on the output bar (Fig. 2), which prevents an unambiguous determination of the later part of compression profile (the dotted line in Fig. 4). Judging by the release in $\bar{\tau}$, however, a rapid unloading was achieved in the experiment. Because the release of frictional sliding was realized through the axial separation of tribo pair while the rotations of the bars were still ongoing, the diminishing of frictional resistance with the disengagement gave rise to an acceleration of the part of specimen bonded to the input bar. This corresponds to the final increase in $\bar{v}$.

Similar dynamic behavior was observed in the other experiments of this series. A summary of the steady-state results obtained is given in Table 1, which is self-explanatory. The steady-state value of $\bar{v}$ was the primary experimental variable of this series of tests. The variations of the other parameters were kept small to reduce the complexity that may arise in interpreting the experimental data. The compression load was controlled so that the variation of plateau $\bar{\sigma}$ is within 8% of the mean value of 175 MPa. The specimens used had essentially the same tribo surface dimensions and surface roughness. The nearly constant $\bar{\sigma}$ and $\bar{\tau}$ in the steady state allow us to use the steady-state nominal kinetic friction coefficient $\bar{\mu}_k = \bar{\tau}/\bar{\sigma}$ as the representative measure for the steady-state response. A plot of $\bar{\mu}_k$ as a function of the (steady-state) nominal sliding velocity is shown in Fig. 5. The data over the range of sliding velocities examined (1.4–6.5 m/s) show a trend of slight decrease in $\bar{\mu}_k$ with increasing sliding velocity. The linear regression (the solid line) of the data gives

Table 1
Summary of experiments and steady-state results on flat-surface tribo pairs

Exp.	Normal stress (MPa)	Steady-state sliding velocity (m/s)	Steady-state kinetic friction coefficient
1	179	1.41	0.167
2	173	2.42	0.170
3	173	2.63	0.143
4	161	3.83	0.137
5	180	4.81	0.160
6	175	5.61	0.137
7	185	6.11	0.105
8	180	6.46	0.121

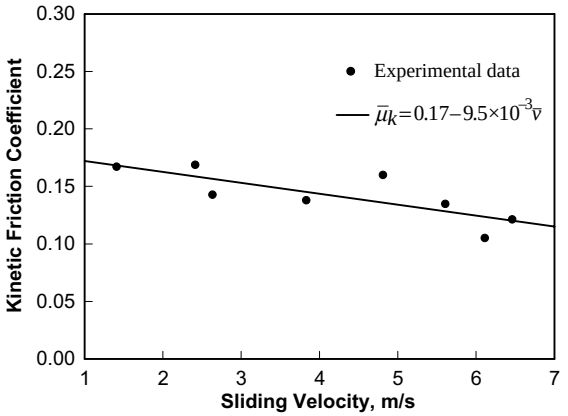

Fig. 5. Steady-state kinetic friction coefficient as a function of sliding velocity. The nominal normal stress variation is within 8% of the mean value (175 MPa).

$\bar{\mu}_k = 0.17$ at a sliding velocity of 1.4 m/s and has a slope of -9.8×10^{-3} s/m. This result is similar to that of the pressure-shear impact experiments by Prakash and Clifton (1993) on flat-surface tribo pairs of SAE 4340 steel and WC/Co tool material. For sliding velocities from 2.5 to 17.5 m/s, they observed a velocity-dependent reduction of kinetic friction coefficient at a rate of 6.8×10^{-3} s/m. However, a significantly stronger velocity dependence was reported by Espinosa et al. (2000) for very low sliding velocities.

3.2. Results on fracture-surface tribo pairs

A series of seven KTB tribometric experiments was conducted on the tribo pairs with as-fractured surfaces. The loading conditions, surface roughness measurements and peak shear stresses are summarized in Table 2. The initial surface roughness of the specimen used in Exp. G is not known because of recording failure of the scanning file. Only the peak-state data will be used in further discussion. The initial sliding velocity will be defined in the next paragraph. Experiments A and B were intended to have the same sliding velocity and Exps. B, C and D to have the same normal stress. Experiments E and F were targeted at a high normal stress. However, in contrast to the high sliding velocity in Exp. E, the interfacial sliding in Exp. F is negligible (if any) as will be demonstrated later. Although all the specimens were prepared in essentially the same way, the initial values of R_v vary from 0.13 to 0.33 mm.

Fig. 6 shows the time history data from Exp. D. Again, it can be seen that the compression loading arrives first and $\bar{\sigma}$ (the solid line with respect to the left axis) reaches its plateau amplitude, 285 MPa in

Table 2
Summary of experiments and results on fracture-surface tribo pairs

Exp.	Normal stress (MPa)	Initial sliding velocity (m/s)	Initial surface roughness (mm)	Peak shear stress (MPa)	Post-test surface roughness (mm)
A	124	1.93	0.158	156	0.129
B	276	1.85	0.129	179	0.090
C	271	3.58	0.290	235	0.208
D	285	3.02	0.330	255	0.252
E	383	3.96	0.231	309	0.159
F	391	–	0.165	319	–
G	250	1.66	–	143	–

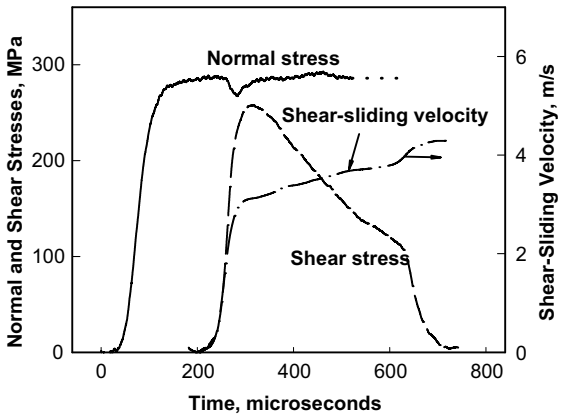

Fig. 6. Typical time-resolved tribometric measurements on closed fracture-surface tribo pair.

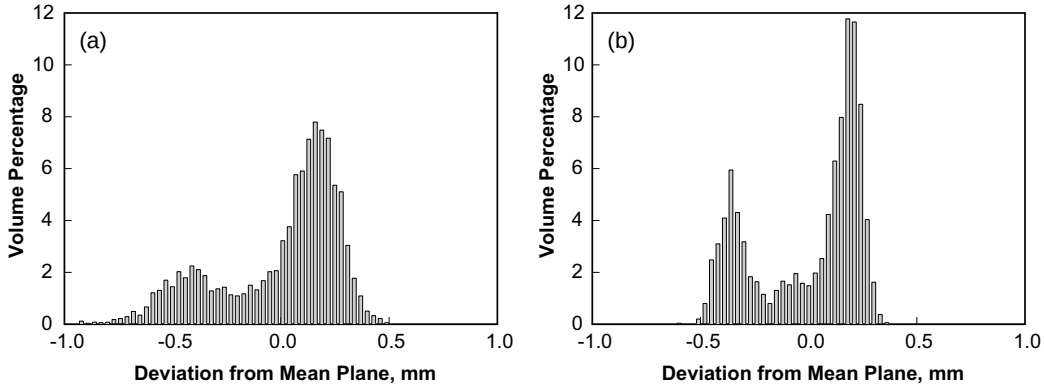

Fig. 7. Statistical asperity spectra of the specimen surface before and after Exp. D: (a) pre-test spectrum and (b) post-test spectrum.

about 100 μs. The shear loading arrives 240 μs later giving rise to a rapid increase in $\bar{v}$ (the dot-dashed line with respect to the right axis) to a value of 3.02 m/s. Afterwards, $\bar{v}$ has a small but noticeable increase with time, which will be discussed later. In response, $\bar{\tau}$ (the dashed line with respect to the left axis) sustained by the closed fracture surface pair increases with the shear velocity up to a peak value of 255 MPa. There is a significant rounding as $\bar{\tau}$ approaches to the peak shear stress $\bar{\tau}_{\max}$ primarily due to progressive yielding of asperities. After a short period of post-peak rounding, the response turns quickly to a rapid decay evolving continuously until the arrival of unloading. The statistical results of 3-D scans of the specimen surfaces before and after this test are shown in Fig. 7. Compared to the as-fractured surface (a), the asperity spectrum of the tested surface (b) is significantly narrower indicating a substantial wear during the experiment. Although plasticity-induced heating may cause thermal softening in the material response, it is not a significant factor for the observed time-dependent decay of $\bar{\tau}$ as will be further discussed later. The decay is due predominantly to surface wear, which must evolve through interfacial sliding. Therefore, as a reasonable approximation, $\bar{v}$ at $\bar{\tau}_{\max}$ can be considered as the initial sliding velocity $\bar{v}_s$ (Column 4 in Table 2). As $\bar{\tau}$ decreases, the angular velocity of input-bar side of specimen accelerates slightly as discussed earlier. This is why $\bar{v}$ is seen to have small but continuous increase after its initial rapid rise. There is a dip in $\bar{\sigma}$ during the rise of $\bar{\tau}$ (Fig. 6). This is due to the dynamics associated with the shear-induced interface

dilatancy. Depending on the level of applied compression, the initial elastic shearing of asperity pairs may cause them to retreat somewhat away from the full engagement giving rise to a momentarily dilated interfacial region with a lower effective mechanical impedance than that of fully engaged interface and consequently a momentary decease in $\bar{\sigma}$. However, both the additional axial wave reverberation triggered by this effective material property change and the plastic shearing of asperities (which reduces the interfacial voids) as the interfacial sliding starts bring $\bar{\sigma}$ quickly back to the plateau resulting in the noticeable but small and rapidly diminishing dip. As described in the previous section, the tribo pair was disengaged by the tensile force resulted from a carefully designed longitudinal wave interaction. The rapid decrease in $\bar{\tau}$ and the sudden increase in $\bar{v}$ indicate the initiation of unloading with the onset of tribo pair disengagement.

Similar dynamic response was observed in the other experiments except for Exp. F, which will be discussed separately. The shear stress histories obtained from Exps. A–E are shown in Fig. 8. Significant decrease of $\bar{\tau}$ with increasing time after an initial peak is apparent for each of the experiments. Overall, $\bar{\tau}_{\max}$ increases with $\bar{\sigma}$ (plateau value) except for Exp. B. The relation between the two is, however, non-linear as will be elaborated later. It is also apparent that the higher the magnitude of $\bar{v}_s$, the stronger the wear-induced decay in $\bar{\tau}$ regardless the values of $\bar{\sigma}$ and $\bar{\tau}_{\max}$. This implies that the post-peak decay is controlled predominantly by $\bar{v}$. It is interesting to see that the values of $\bar{\tau}$ right before the unloadings in Exps. B–D (with nearly the same $\bar{\sigma}$) are approximately the same even though the values of $\bar{\tau}_{\max}$ and the trends of decay (wear process) are very much different from one to another. This means that $\bar{\tau}$ will reach a rather steady state if the loading period is sufficient long. The evolution of fracture surface roughness plays an important role only in the process leading to this steady state.

In contrast, as shown in Fig. 9, the $\bar{\tau}$ data from Exp. F (the solid line) are qualitatively different from those in Fig. 8. There is no decay in $\bar{\tau}$ between its initial rise and unloading. Instead, there is a small but noticeable continuous increase in $\bar{\tau}$ after the rise time, in other words, a sign of strain hardening. The loading condition of the experiment was such that the plateau $\bar{\sigma}$ was as high as 391 MPa and that of $\bar{v}$ was as low as 0.8 m/s. It is likely that the high normal stress suppressed the occurrence of frictional sliding, which would have been quite small if existed, to allow the material in the vicinity of the interface to undergo a dynamic plastic deformation continuous across the interface. The estimated shear

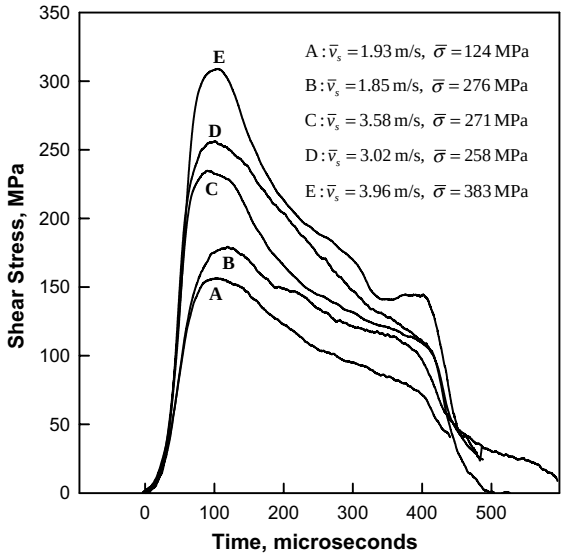

Fig. 8. Shear stress histories for various shear-sliding velocities, normal stresses and initial values of roughness.

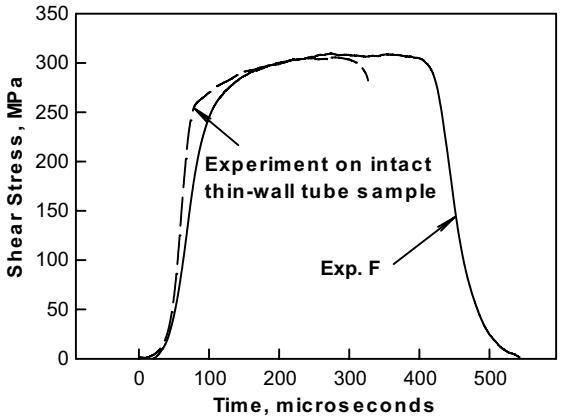

Fig. 9. Comparison of the dynamic shear response of a closed 7075-T6 fracture surface pair under high normal stress and that of an intact thin-wall tube specimen of the same material at a shear rate of 3600 1/s.

strain rate assuming no sliding is in the range from 1600 to 2700 s^{-1} depending on the width of plastic deformation zone (0.3–0.5 mm). An additional KTB experiment using a standard (intact) thin-wall tube specimen was conducted for comparison. A shear rate of 3600 s^{-1} was reached in the experiment. The shear stress history before a localized failure is also shown in Fig. 9 as the dashed line. In terms of peak shear stress, the two results are very close. Indeed, the response measured in Exp. F is that of dynamic plasticity without interfacial sliding. A low shear velocity is also critical to this transition since significant frictional sliding occurred in Exp. E under a similar $\bar{\sigma}$ (383 MPa) but a much higher peak shear velocity (3.96 m/s). However, in a shear cracking process, a high fracture-surface sliding velocity can be achieved only after substantial crack propagation. At the initiation stage of crack propagation, the loading condition on the fractured surfaces is much closer to that of Exp. F than that of Exp. E. It can therefore be concluded that a sufficiently high *confining* stress may suppress further cracking in a metallic solid containing interior cracks and effectively restore the macroscopic material strength. Furthermore, the results shown in Fig. 9 indicate that the thermal softening of material response due to the plasticity-induced, nearly adiabatic heating in these experiments is not sufficient to overwhelm the strain hardening. This supports the conclusion that thermal softening is not a significant factor for the shear stress decay seen in Figs. 6 and 8.

In Fig. 10, the values of measured $\bar{\tau}_{\max}$ are plotted against the corresponding plateau values of $\bar{\sigma}$ for Exps. A–G. The relationship is clearly non-linear. The highest $\bar{\tau}_{\max}/\bar{\sigma}$ ratio occurs actually at the lowest $\bar{\sigma}$ (124 MPa). A jump-like response appears around $\bar{\sigma} = 280$ MPa. The dashed line in the figure indicates the peak flow stress measured in the aforementioned standard KTB experiment, which is very close to the $\bar{\tau}_{\max}$ value obtained in Exp. E. Clearly, the material shear strength sets a limiting stress for the frictional response of the fracture surface pairs. As $\bar{\tau}_{\max}$ approaches the limit stress, a transition from frictional sliding with asperity wear (localized plasticity) to macroscopic plastic flow takes place. However, as indicated by the later-time response of Exp. E (Fig. 8), the transition reverses once interfacial sliding occurs. As long as there exists interfacial sliding, surface wear through localized plastic deformations at asperity tips dominates the tribo pair response even if $\bar{\tau}$ reaches the limit stress temporarily. This is the case for all the fracture surface experiments except for Exp. F, where the transition sustained throughout the experiment. The lack of consistent correlation between $\bar{\tau}_{\max}$ and $\bar{\sigma}$ indicates that in addition to $\bar{\sigma}$, $\bar{\tau}_{\max}$ is also significantly influenced by at least one of the other parameters. The one comes to immediate attention is the initial value of R_v. It is found that the following non-linear scaling:

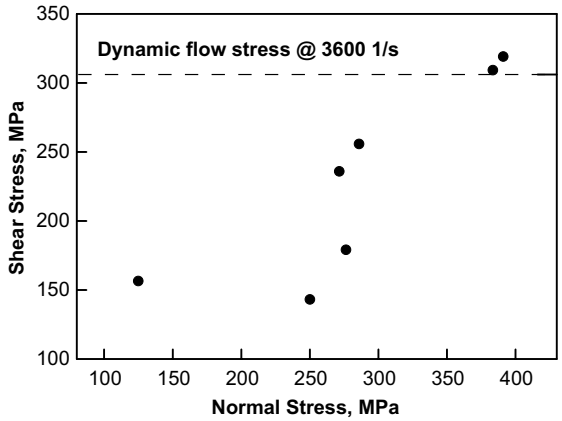

Fig. 10. Peak shear stress as a function of normal stress (different initial values of fracture surface roughness). The dashed line indicates the material shear strength at the shear rate of 3600 1/s.

$$T_{\max} \equiv \bar{\tau}_{\max}/(R_v/R_0)^{0.35} \tag{4}$$

with $R_0 = 1$ mm has a much more consistent correlation with $\bar{\sigma}$ as shown in Fig. 11. In fact, the relationship between the scaled peak stress $T_{\max}$ and $\bar{\sigma}$ can be well approximated with the following exponential function:

$$T_{\max} = a + b\exp(c\bar{\sigma}), \tag{5}$$

where $a = 273$ MPa, $b = 8.13$ MPa, and $c = 8.87 \times 10^{-3}$ $(\text{MPa})^{-1}$. The result of Eq. (5) is plotted in Fig. 11 as the solid line.

The results presented so far show little influence of $\bar{v}$ on the peak-state response of the fracture surface pairs. Furthermore, its influence on the post-peak decay of $\bar{\tau}$ (Fig. 8) may more reasonably be considered as through the sliding displacement. As an examination of this view point, the decays measured in Exps. A–E are plotted in Fig. 12 in terms of $\bar{\tau}$ vs. the nominal shear displacement s (time integration of $\bar{v}$), which is the sum of non-sliding displacement s' and sliding displacement $s - s'$. Indeed, the post-peak $\bar{\tau} - s$ profiles (the

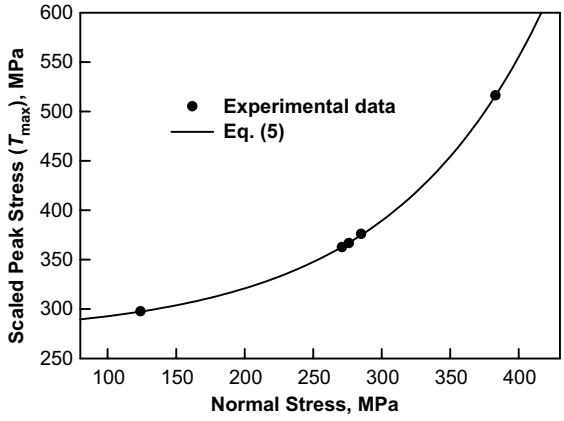

Fig. 11. Scaled peak stress as a function of normal stress.

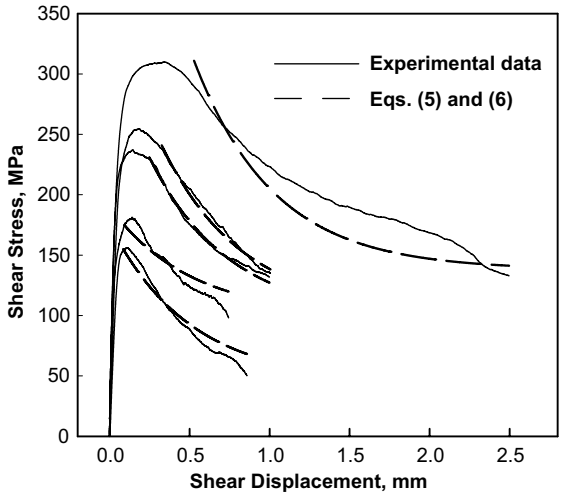

Fig. 12. Comparison of model calculations with experimental data.

solid lines) are quite similar in terms of the decay trend. The reduction rate of each of the profiles resembles that of a three-parameter exponential decay. This observation motivates the following empirical model:

$$\bar{\tau} = \mu\bar{\sigma} + [T_{\max}(R_v/R_0)^{0.35} - \mu\bar{\sigma}] \exp\left(-\frac{s - s'}{\lambda}\right), \tag{6}$$

where $T_{\max}$ is given by Eq. (5), and μ and λ are two model parameters. Specifically, μ measures the assumed linear dependence of steady-state response on $\bar{\sigma}$, and λ controls the transient behavior between the peak and steady state. The results of Eqs. (5) and (6) with $\mu = 0.36$ and $\lambda = 0.5$ mm are also shown in Fig. 12 as the dashed lines. Though overestimating the decay in Exp. E somewhat, the simple model does a quite good job in capturing the essential features of the experimental results considering the complexity of the data. Because the model was derived empirically from limited experimental observations and data, its validity for conditions beyond what have been examined in this work is not clear. Caution needs to be exercised for such an extension.

It should be pointed out that the KTB tribometric experiment presented above is for measuring the transient response of tribo pairs under impulsive loading and nearly adiabatic condition. The typical time duration of combined compression and shear used is approximately 250 μs. Longer durations are possible but practically limited to a time scale within 1 ms. Although the attainment of steady state has been routinely observed if wear-induced interface evolution during the experiment is minimal as in the case of the tests on the flat surface pairs (Fig. 4) or diminishes with increasing sliding distance as found for ceramic surface pairs (the results of which will be reported separately), it is possible that the interface evolution remains significant throughout the duration of experiment thus preventing the attainment of steady state as in the case of the tests on the fracture surface pairs (Fig. 8). In such a scenario, the time history data from the KTB tribometry and the quantitative characterization of initial and as-tested surfaces may permit a reasonable prediction of the steady-state response in conjunction with proper modeling if the predominant wear mechanism is essentially stress-dependent and insensitive to relatively small temperature variation as it is for the current case. However, the technique used in this work may not be appropriate for characterizing the tribological response involving wear mechanisms that depend strongly on repetitive loading, e.g., fatigue, very slow processes such as oxidization, and/or on relatively small variation of surface temperature.

4. Conclusions

The Kolsky (split-Hopkinson) torsion bar technique has been utilized successfully to develop a new compression-shear recovery experiment for dynamic tribometry of closed fracture surface pairs. This new experimental design enables combined dynamic compression and shear loading and preserves the residual specimen surface after a well-defined single cycle of loading. The technique complements that of the pressure-shear plate impact experiment in that the applied compression and shear can be controlled fully independently for compressive forces up to 20 kN and shear velocities up to 10 m/s, and in that the specimen can be easily recovered after a single loading cycle. The latter permits meaningful comparison between the initial and tested surfaces of the specimen.

The experimental design has been verified in a series of tribometric tests on flat-surface tribo pairs of 7075-T6 Al. Clean and repeatable measurements were obtained and the specimen recovery after a single loading cycle was demonstrated. The experimental results show that except for a small and rapidly diminishing initial peak, the dynamic frictional response of the flat-surface tribo pairs is essentially Coulombic with a very weak dependence on the sliding velocity for the range of sliding velocities examined (1.4–6.5 m/s). This is consistent with the dynamic friction measurements reported in the literature for flat-surface metallic tribo pairs under similar sliding velocities.

The technique has been applied to study the dynamic tribological response of closed fracture surface pairs of 7075-T6 Al in conjunction with non-contact 3-D profilometry of the initial and tested specimen surfaces. It was found that the pre-sliding response depends primarily on applied normal stress and roughness of as-fractured surface. The response immediately after the initiation of frictional sliding displays, however, an exponential-decay-like softening with increasing sliding displacement. This has been identified, through the comparison of pre- and post-test surface topography measurements, to be the result of interface wear in the form of asperity shearing. The long-time steady-state response (if achieved) depends predominantly on normal stress. The results also show that a sufficiently high normal stress may suppress frictional sliding between the closed fracture surfaces giving rise to a dynamic plastic deformation continuous across the interface. It is therefore possible to use high confining stress suppressing further cracking in a metallic solid having pre-exiting interior cracks and restoring effectively the macroscopic material strength. A simple empirical model is proposed and evaluated against the experimental data. It is demonstrated that the model captures the key features of observed dynamic tribological response of the closed fracture surface pairs.

A similar study on the dynamic tribological response of closed ceramic fracture surface pairs has also been carried out. The results will be reported separately.

Acknowledgements

The materials reported in this paper are from the work supported by the US Army Research Office through Grant No. DAAD19-99-1-0117 (Project Manager: Dr. B. LaMattina). Y. Hu is thanked for providing assistance in conducting the experiments.

References

Espinosa, H.D., 1995. On the dynamic shear resistance of ceramic composites and its dependence on applied multiaxial deformation. Int. J. Solids Struct. 32, 3105–3128.

Espinosa, H.D., Patanella, A., Fisher, M., 2000. A novel dynamics friction experiment using a modified Kolsky bar apparatus. Exp. Mech. 40, 138–153.

Hartley, K.A., Duffy, J., Hawley, R.H., 1985. The torsional Kolsky (split-Hopkinson) bar. ASM Metals Handbook, 43, ASM International, Metals Park, Ohio, pp. 218–228.

Lindholm, U.S., 1964. Some experiments with the split Hopkinson pressure bar. J. Mech. Phys. Solids 12, 317–335.

Margolin, L.G., 1984. Microphysical models for inelastic material response. Int. J. Eng. Sci. 22, 1171–1179.

Ogawa, K., 1997. Impact friction test method by applying stress waves. Exp. Mech. 37, 398–402.

Prakash, V., 1995. A pressure-shear plate impact experiment for investigating transient friction. Exp. Mech. 35, 329–336.

Prakash, V., Clifton, R.J., 1993. Time resolved dynamic friction measurements in pressure shear. In: Ramesh, K.T. (Ed.), Experimental Techniques in the Dynamics of Deformable Solids. ASME, New York, pp. 33–48.

Rajagopalan, S., Prakash, V., 1999. A modified torsional Kolsky bar for investigating dynamic friction. Exp. Mech. 39, 295–303.

Rajendran, A.M., 1994. Modeling the impact behavior of AD85 ceramic under multiaxial loading. Int. J. Imp. Eng. 15, 749–768.

Suh, N.P., 1986. Tribophysics. Prentice-Hall, New Jersey.

Theocaris, P.S., Panagiotopoulos, P.D., Bisbos, C., 1993. Unilateral contact, friction and related interactions in cracks: The direct boundary integral method. Int. J. Solids Struct. 30, 1545–1561.

Wright, T.W., 1998. A note on frictional release in microcracks. Int. J. Fract. 91, L37–L42.